Coupling Strategy for Resolving In-duct Elastic Panel Aeroacoustic-Structural Interaction with CE/SE Method

Harris K. H. Fan[1], Randolph C. K. Leung[2], and Garret C. Y. Lam[3]
The Hong Kong Polytechnic University, Hung Hum,

Kowloon, Hong Kong, People's Republic of China

Yves Aurégan[4] and Xiwen Dai[5]
LAUM, UMR CNRS 6613, Av. O Messiaen, F-72085 LE MANS Cedex 9, France

Nomenclature

C = structural damping coefficient

$\hat{c}_0$ = reference acoustic speed in unit of m/s

$\hat{c}_p$ = specific heat capacity

D = bending stiffness

E = total energy

E_p = modulus of elasticity

f = frequency

H = duct width

h_p = thickness of panel

K_p = stiffness of foundation supporting the panel

k = thermal conductivity

[1] PhD Candidate, Department of Mechanical Engineering, email address: harris-ka-heng.fan@polyu.edu.hk.
[2] Associate Professor, Department of Mechanical Engineering, email address: mmrleung@polyu.edu.hk, Senior Member AIAA.
[3] Research Associate, Department of Mechanical Engineering, email address: garret.lam.hk@connect.polyu.hk.
[4] Research Director, CNRS, email address: yves.auregan@univ-lemans.fr.
[5] Postdoctoral Researcher, LAUM, email address: xiwen.dai@univ-lemans.fr.

$\hat{L}_0$ = reference length in unit of m

L_d, L_u = duct lengths of panel downstream and upstream

L_p = length of panel

l = height of a fluid control volume

M = Mach number

N_{iter} = number of iteration

N_x = internal tensile stress

Pr = Prandtl number

p = pressure

p_{ex} = net pressure exerted on the panel surface

q_x, q_y = heat flux in x and y directions

$\hat{R}$ = specific gas constant for air in unit of $\mathrm{J/(kg \cdot K)}$

Re = Reynolds number

$\hat{T}_0$ = reference temperature in unit of K

T_{comp} = wall-clock time

T_x = external tensile stress

TL = transmission loss

t = time

U = inlet flow speed

u, v = velocity in x and y directions

u_0 = mean flow speed

w = panel displacement

γ = specific heat ratio

Δt = time step size

δ = initial undeflected height of a fluid control volume

ϵ = precision requirement

λ = relaxation factor

μ = viscosity

ρ = density of fluid

$\hat{\rho}_0$ = reference density in unit of kg/m^3

ρ_p = density of panel

σ = total stress at the fluid-panel interface

τ_{xx}, τ_{yy} = normal stress in x and y directions

τ_{xy} = shear stress

Subscript

H = homogeneous solution

a = above the panel

b = below the panel

j = number of time step

k = number of iteration step

panel = at the fluid-panel interface

Superscript

$\hat{}$ = dimensional variable

I. Introduction

Accurate prediction of complex interaction of noise and flow-induced vibration has been a challenging task in devising aeroacoustic control for flow ducts installed in such engineering applications as ventilation in air-/land- transportation vehicles and extensive compressed gas transportation networks, etc. The structural configurations of the ducts in these applications are so designed that their walls are considered effectively elastic. As such they are easily excited to vibrate by the unsteady duct flow and the noise it carries. The vibrating duct walls will then generate additional flow disturbances to modify the flow in their vicinity and radiate extra noise to both interior and exterior of flow ducts. It is not difficult to see that a complex interplay between unsteady flow, noise scattering, as well as duct wall dynamics prevails which determines the ultimate level of noise propagating to duct far downstream. Such complex interplay is termed as aeroacoustic-structural

interaction (AASI) [1] because the unsteady flow, acoustics and structural dynamics contribute equally in a fully coupled manner. A lack of the understanding of its physics makes the prediction of eventual noise amplification and/or reduction extremely difficult, not to mention the development of an effective aeroacoustic control design for flow duct.

Measurement of AASI of an elastic panel is a very difficult task as the problem involves the mutual interaction of panel bending waves with nonlinear scale-disparate flow motions. This fact renders the popularity of AASI studies by means of time-domain numerical approaches in literature and many numerical strategies that couple the flow and panel dynamic solutions were attempted. For example, Lucey and Carpenter [2] investigated theoretically the hydroelastic stability of a finite compliant panel under unsteady potential flow. The critical flow speed for the onset of instability is predicted. The influence of the panel width on the critical vibration mode and the panels array on the stability are also studied. Sucheendran et al. [3] studied the structural-acoustic response of a thin plate flush-mounted in a rectangular duct and subjected to grazing incident acoustic waves and subsonic uniform mean flow. They revealed that strong interaction arises for relatively soft and thin plate and heavy fluid loading. Besides, Vitiello et al. [4] developed a numerical procedure to study the response of a plate excited by turbulent flow. The significance of effect of flow on the plate is highlighted. Schäfer et al. [5] simulated the acoustic waves radiated from a vibrating thin plate excited by a low subsonic turbulent flow. Although the dominated structural and acoustic responses were captured well compared to the experimental data, an appropriate damping model for high frequencies, which is not easy to determine, was required for more realistic simulation. Recently, Shishaeva et al. [6] studied and revealed three kinds of nonlinear unstable behavior, divergence, single- and coupled-mode flutters, of a plate in the low supersonic inviscid flow with different Mach numbers.

We are particularly interested in a duct noise control concept, panel muffler, proposed by Huang [7] in which the control is facilitated by the acoustically induced vibration of an elastic panel flush-mounted in a rigid duct. Fan et al. [1] attempted to numerically resolve the aeroacoustic-structural responses of this problem under inviscid flow assumption and proved the same configuration a promising aeroacoustic control design with duct flow over a wide range of Mach numbers.

However, in practical situations, the fluid viscosity may play a significant role in the interaction due to additional shear stresses applied on the panel. It may also enhance the perturbation level of the flow over the vibrating panel which may consequently amplify the vibration. There were attempts in resolving viscous interaction between civil engineering structures and incompressible flows [8, 9] using finite element method. The authors compared the accuracy of solution time marching obtained from partitioned and monolithic fluid-structure coupling schemes. Their results showed that the partitioned scheme was not good at solving strong flow-structure interaction but there was room for improvement of solution accuracy with monolithic scheme. However, there was another study that involved the use of partitioned scheme for solving the nonlinear flow-structure interaction of an elastic panel exposed to flows at low supersonic speeds [6]. Multiple modes of panel flutter were successfully captured. None of these studies explicitly involves acoustics in the problem and the suitability of both schemes in resolving in-duct aeroacoustic-structural interaction is still in question. This Technical Note attempts to address this question by examining the accuracy of and calculation time required for solution time marching with selected in-duct aeroacoustic-structural interaction problems of various complexity. Comparisons with existing experimental data, theoretical and numerical solutions of the selected problems are made.

II. Problem of Interest and Physical Models

The physical problem of interest is the aeroacoustic-structural interaction emerging in the drum-like silencer configuration [10] where two elastic panels backed by cavities are flush-mounted face-to-face in an infinitely long rigid duct (Figure 1). The cavities are introduced to enhance the impedance mismatch above the panels and thus the transmission loss of the silencer at low frequencies and block the acoustic wave radiating to duct exterior. In essence, an acoustic wave propagates along the duct and excites the panels to vibrate. The induced panel vibration creates impedance mismatch, reflects the incident acoustic wave and modify the dynamics of flow in its vicinity. For the sake of simplicity, the analysis of noise reduction is carried out by assuming a two dimensional domain and a one dimensional panel (i.e. a beam) structure [7]. In the forthcoming discussions all the variables mentioned in the rest of the paper are normalized by a reference length $\hat{L}_0 = \hat{L}_p$, a reference density

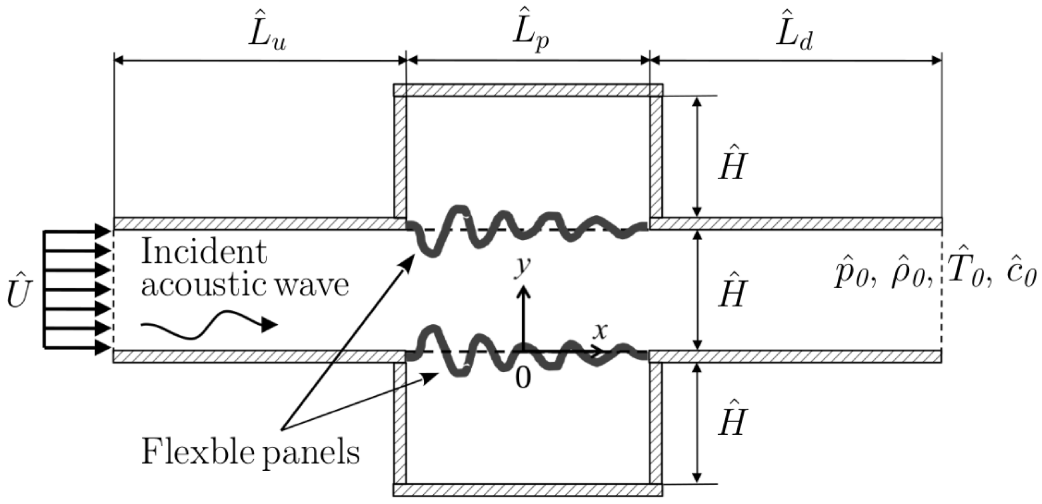

Fig. 1 The schematic configuration of the drumlike silencer concept (not-to-scale).

$\hat{\rho}_0$ and a reference acoustic speed $\hat{c}_0$.

The aeroacoustic response is modeled by solving the two dimensional compressible Navier-Stokes (N-S) equations together with the ideal gas law for calorically perfect gas. The normalized governing equations can be written in the strong conservation form as,

$$\frac{\partial \boldsymbol{U}}{\partial t} + \frac{\partial \left(\boldsymbol{F} - \boldsymbol{F}_v\right)}{\partial x} + \frac{\partial \left(\boldsymbol{G} - \boldsymbol{G}_v\right)}{\partial y} = 0, \tag{1}$$

where $\boldsymbol{U} = [U_1,\ U_2,\ U_3,\ U_4]^\intercal = [\rho,\ \rho u,\ \rho v,\ \rho E]^\intercal$, $\boldsymbol{F} = \left[\rho u,\ \rho u^2 + p,\ \rho uv,\ (\rho E + p)u\right]^\intercal$, $\boldsymbol{G} = \left[\rho v,\ \rho uv,\ \rho v^2 + p,\ (\rho E + p)v\right]^\intercal$, $\boldsymbol{F}_v = (M/Re)\,[0,\ \tau_{xx},\ \tau_{xy},\ \tau_{xx}u + \tau_{xy}v - q_x]^\intercal$, $\boldsymbol{G}_v = (M/Re)\,[0,\ \tau_{xy},\ \tau_{yy},\ \tau_{xy}u + \tau_{yy}v - q_y]^\intercal$, $\rho = \hat{\rho}/\hat{\rho}_0$ is the density of fluid, $u = \hat{u}/\hat{c}_0$ and $v = \hat{v}/\hat{c}_0$ are the velocities in $x = \hat{x}/\hat{L}_0$ and $y = \hat{y}/\hat{L}_0$ directions respectively, $t = \hat{t}\hat{c}_0/\hat{L}_0$ is the time, the total energy $E = \hat{E}/\hat{c}_0^2 = p/[\rho(\gamma - 1)] + (u^2 + v^2)/2$, the pressure $p = \hat{p}/(\hat{\rho}_0\hat{c}_0^2) = \rho T/\gamma$, the normal and shear stresses $\tau_{xx} = (2/3)\mu[2(\partial u/\partial x) - (\partial v/\partial y)]$, $\tau_{yy} = (2/3)\mu[2(\partial v/\partial y) - (\partial u/\partial x)]$ and $\tau_{xy} = \mu[(\partial u/\partial y) + (\partial v/\partial x)]$, $\mu = \hat{\mu}/\hat{\mu}_0$ is the viscosity, the heat fluxes $q_x = -k(\partial T/\partial x)/[(\gamma - 1)Pr]$ and $q_y = -k(\partial T/\partial y)/[(\gamma - 1)Pr]$, the thermal conductivity $k = \mu\hat{c}_p/Pr$, the specific heat capacity $\hat{c}_p = \gamma\hat{R}/(\gamma - 1)$, the specific heat ratio $\gamma = 1.4$, the specific gas constant for air $\hat{R} = 287.058$ J/(kg $\cdot$ K), Prandtl number $Pr = \hat{c}_p\hat{\mu}_0/\hat{k}_0 = 0.71$, Mach number $M = \hat{u}_0/\hat{c}_0$, Reynolds number $Re = \hat{\rho}_0\hat{u}_0\hat{L}_0/\hat{\mu}_0$, $\hat{u}_0$ is the mean flow speed, the acoustic speed $\hat{c}_0 = \sqrt{\gamma\hat{R}\hat{T}_0}$ and the reference temperature $\hat{T}_0 = 288.2$ K. For inviscid flow, the viscous terms are ignored so that

$\boldsymbol{F}_v = \boldsymbol{G}_v = 0$.

The elastic panel is assumed to be of uniform small thickness $h_p = \hat{h}_p/\hat{L}_p$ and initially flat. Its nonlinear dynamic response can be modeled by solving the one dimensional plate equation to the simplest approximation [11]. The normalized governing equation for panel displacement $w(x) = \hat{w}/\hat{L}_0$ can be written as,

$$D\frac{\partial^4 w}{\partial x^4} - (T_x + N_x)\frac{\partial^2 w}{\partial x^2} + \rho_p h_p \frac{\partial^2 w}{\partial t^2} + C\frac{\partial w}{\partial t} + K_p w = p_{ex}, \tag{2}$$

where $N_x = (E_p h_p/2L_p)\int_0^{L_p} (\partial w/\partial x)^2\, dx$ is the internal tensile stress in the tangential direction induced by stretching, $D = \hat{D}/(\hat{\rho}_0 \hat{c}_0^2 \hat{L}_0^3)$ is the bending stiffness, $T_x = \hat{T}_x/(\hat{\rho}_0 \hat{c}_0^2 \hat{L}_0)$ is the external tensile stress resultant per unit length in tangential direction (i.e. x-direction), $E_p = \hat{E}_p \hat{c}_0^2/(\hat{\rho}_0 \hat{L}_0^4)$ is the modulus of elasticity, $L_p = \hat{L}_p/\hat{L}_0$ is the length of panel, $\rho_p = \hat{\rho}_p/\hat{\rho}_0$ is the density of panel, $C = \hat{C}/(\hat{\rho}_0 \hat{c}_0)$ is the structural damping coefficient, $K_p = \hat{K}_p \hat{L}_0/(\hat{\rho}_0 \hat{c}_0)$ is the stiffness of foundation supporting the panel and $p_{ex} = \hat{p}_{ex}/(\hat{\rho}_0 \hat{c}_0^2)$ is the net pressure exerted on the panel surface.

III. Strategies for Aeroacoustic-Structural Coupling

A. Partitioned Coupling Scheme

The partitioned coupling scheme calculates the aeroacoustics and panel dynamics using individual solvers separately, with respective instantaneous boundary conditions, and allows their communication by a one after another coupling strategy. Fan et al. [1] showed the partitioned scheme can accurately resolve the aeroacoustic-structural responses of the elastic panels exposed to duct flow. They solved the aeroacoustic and panel dynamic responses with conservation element and solution element (CE/SE) and finite difference methods respectively. The panel force exerted on the aeroacoustic domain take effect by setting the boundary condition on the fluid-panel interface through the corresponding ghost points. As shown in Figure 3(b), the ghost point A_G are artificial solution points as mirror images to boundary solution point A_B. Through an interpolation between A_B and A_G, appropriate flow variables are specified at the ghost cell to account the flow conditions given by the panel response at the fluid-panel interface. The detail of the setting of ghost points can be referred in the work of Fan et al. [1]. Since the fluid and panel dynamics are calculated separately, one response always lags another by a time step. Fan et al. [1] developed an iterative

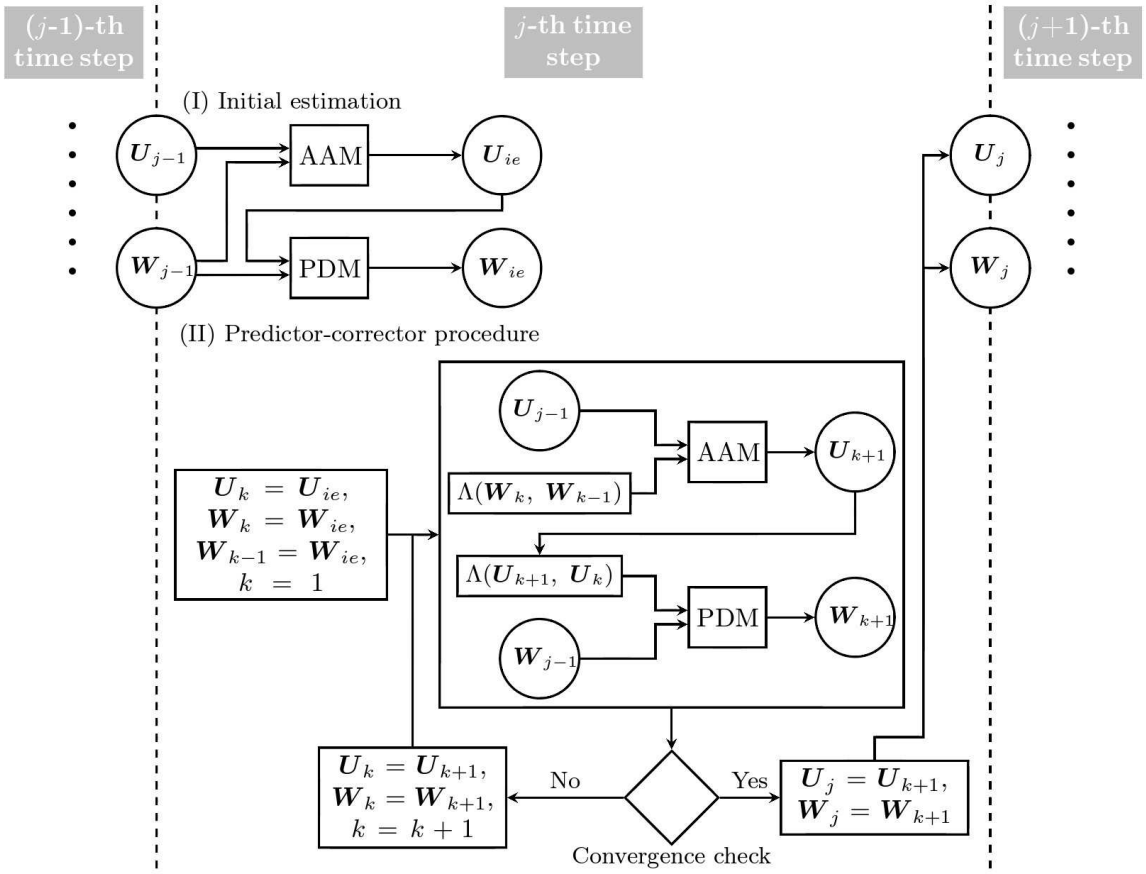

Fig. 2 Iterative correction procedure in the partitioned coupling scheme [1]. AAM, aeroacoustic model; PDM, panel dynamic model. $\boldsymbol{W} = [w,\ \dot{w},\ \ddot{w}]$ is panel vibration response. The function $\Lambda(X_1,\ X_0) = \lambda X_1 + (1-\lambda)X_0$ where λ is the relaxation factor.

correction procedure (Figure 2) to reduce the error due to the lagging so that the simultaneous interaction between two responses are properly resolved. They established the effectiveness of the procedure with calculations of transmission loss created by drumlike silencers with various structural damping settings in the absence of flow. Excellent agreement with theory was obtained. They proceeded with the established numerical procedure to study the aeroacoustic-structural interaction arising from an acoustic wave convecting with a duct flow from low subsonic to low supersonic Mach numbers. Their results firmly reveal the critical role of flow Mach number in aeroacoustic-structural interaction in which the transmission loss is found reducing from more than 20 dB down to 0 dB as Mach number increases while the acoustic wave was propagating along the flow. Transmission loss goes up again with supersonic flow due to the emergence of weak shock waves and their interaction

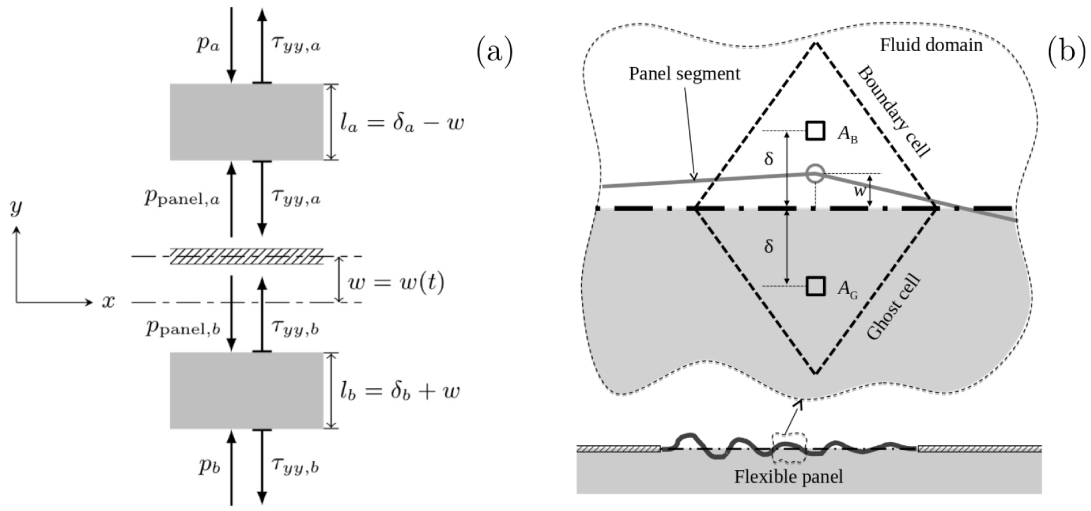

Fig. 3 (a), free-body diagram of fluid control volumes width Δx, and (b), setting of mesh points above and below elastic panel segment as in Fan et al. [1] (not-to-scale).

with the panel [1].

B. Monolithic Coupling Scheme

The monolithic coupling scheme treats the fluid-panel system as a single entity and solves the aeroacoustic and panel dynamic responses simultaneously in a tightly coupled manner (i.e. no lagging in a time step). In essence, only one set of governing equations are developed that inherently facilitate the communication of aeroacoustic and panel dynamic responses.

1. Coupled fluid-panel equation

Consider the stresses experienced by two small control volumes of fluid above and below an elastic panel segment as shown in Figure 3(a). As the vertical vibration of the panel is the primary interest (i.e. Equation 2) in the present study so only the stresses acting on the control volumes along y-direction are considered. The initial undeflected height of each control volume is δ. The vibratory displacement $w(t)$ of the panel segment compresses/stretches the control volumes above/below it during fluid-panel interaction and the height of each control volume, $l(t) = \delta - w(t)$, varies temporally as a result. As we primarily focus on weak panel vibration responses such that $w < \delta$ so the condition $l_a(x,t) + l_b(x,t) = \delta_a(x,0) + \delta_b(x,0)$ holds along entire panel. For a flow past a stationary rigid

boundary, the normal stress induced by fluid viscosity action on each control volume can be expressed as $\tau_{yy} = (2/3)\mu\,[2(\partial v/\partial y) - (\partial u/\partial x)]$ [12] which may be further simplified as $\tau_{yy} = (4/3)\mu(\partial v/\partial y)$ when no-slip boundary condition (i.e. $\partial u/\partial x = 0$) on panel surface is assumed. When a fluid volume is compressed/stretched by panel displacement, an additional stress $\sigma = \tau_{yy} - p$ is created at the fluid-panel interface whose gradient is given by

$$\frac{\partial \sigma}{\partial y} = \frac{\partial \tau_{yy}}{\partial y} - \frac{\partial p}{\partial y} \approx -\frac{\partial p}{\partial y}.$$

Since the magnitude of viscous stress gradient $\partial \tau_{yy}/\partial y = (4/3)\mu(\partial^2 v/\partial y^2)$ is two orders of magnitude weaker than that of pressure gradient $\partial p/\partial y$, it can be neglected for convenience so $\partial \sigma/\partial y \approx -\partial p/\partial y$. Subsequently the mechanical power per unit length produced by σ is thus given by [12],

$$v\frac{\partial \sigma}{\partial y} \approx -v\frac{\partial p}{\partial y}.$$

The stress σ arising from the vibrating fluid-panel interface injects, or consumes, additional momentum and energy to fluid domain. One convenient way to resolve its effects due to aeroacoustic-structural interaction at the fluid-panel interface is to include them in a source term $\boldsymbol{Q}$ on the right hand side of the aeroacoustic model (i.e. Equation 1) which may now take an inhomogeneous form as

$$\frac{\partial \boldsymbol{U}}{\partial t} + \frac{\partial \left(\boldsymbol{F} - \boldsymbol{F}_v\right)}{\partial x} + \frac{\partial \left(\boldsymbol{G} - \boldsymbol{G}_v\right)}{\partial y} = \boldsymbol{Q}, \tag{3}$$

where

$$\boldsymbol{Q} = \begin{cases} [Q_1,\ Q_2,\ Q_3,\ Q_4]^{\intercal} = -\dfrac{\partial p}{\partial y}\,[0,\ 0,\ 1,\ v]^{\intercal}, & \text{along fluid-panel interface,} \\ 0, & \text{elsewhere.} \end{cases} \tag{4}$$

One should note that all the elements of $\boldsymbol{Q}$ are inherently dependent on panel dynamics. The net external force per unit length applied to the panel is $p_{ex} = \sigma_{\text{panel},b} - \sigma_{\text{panel},a} = (p_{\text{panel},b} - \tau_{yy,b}) - (p_{\text{panel},a} - \tau_{yy,a})$. In order to satisfy the tangency condition at the fluid-panel interface, the velocity in y-direction on either side of the panel

$$v = \frac{\partial w}{\partial t} + u\frac{\partial w}{\partial x} = \frac{\partial w}{\partial t}. \tag{5}$$

The convective term $u\partial w/\partial x$ takes effect only for sliding wall condition in inviscid flow ($u \neq 0$ on walls). However, this is not the situation in all cases reported in the forthcoming discussions so the term is ignored. For a small fluid volume flowing at a low velocity ($M < 0.3$), the local viscous and compressibility effects can be ignored to the first order [13]. Consequently, the normal pressure gradient and the panel acceleration are connected through momentum equation, i.e.,

$$\frac{\partial p}{\partial y} = -\rho \frac{\partial v}{\partial t} = -\rho \frac{\partial^2 w}{\partial t^2}, \tag{6}$$

which essentially provides a dynamical relationship for the inhomogeneous aeroacoustic model (Equation 3) and the panel dynamic model (Equations 2) to couple and communicate.

2. Solution of coupled equation and discretization

The source term $\boldsymbol{Q}$ is a function of the solution vector $\boldsymbol{U}$ so the coupled fluid-panel equation (3) cannot be solved explicitly. Therefore an iterative procedure based on the principle given by Loh [14] is developed to solve for $\boldsymbol{U}$. First, $\partial \boldsymbol{U}/\partial t$ in Equation 3 can be expressed as,

$$\frac{\partial \boldsymbol{U}}{\partial t} = \boldsymbol{Q} - \boldsymbol{H'}, \qquad \boldsymbol{H'} = \frac{\partial \left(\boldsymbol{F} - \boldsymbol{F}_v\right)}{\partial x} + \frac{\partial \left(\boldsymbol{G} - \boldsymbol{G}_v\right)}{\partial y}. \tag{7}$$

At j-th time step of solution time marching, an approximation $\partial \boldsymbol{U}/\partial t \approx (\boldsymbol{U}_j - \boldsymbol{U}_{j-1})/\Delta t$ can be invoked so the solution vector can be estimated as

$$\boldsymbol{U}_j = \Delta t \left(\boldsymbol{Q}\left(\boldsymbol{U}_j\right) - \boldsymbol{H'}\right) + \boldsymbol{U}_{j-1}. \tag{8}$$

To eliminate $\boldsymbol{H'}$, the local homogeneous solution $\boldsymbol{U}_{j,H}$ when $\boldsymbol{Q} = 0$ is separately determined as,

$$\boldsymbol{U}_{j,H} = \boldsymbol{U}_{j-1} - \Delta t \boldsymbol{H'}. \tag{9}$$

Eliminating $\boldsymbol{H'}$ from Equations 8 and 9 results in the equation

$$\boldsymbol{U}_j - \Delta t \boldsymbol{Q}\left(\boldsymbol{U}_j\right) - \boldsymbol{U}_{j,H} = \boldsymbol{\Phi}\left(\boldsymbol{U}_j\right) = 0, \tag{10}$$

The solution $\boldsymbol{U}_j$ of this implicit equation is solved with Newton's method through iterating the following equation,

$$\boldsymbol{U}_{j,k+1} = \boldsymbol{U}_{j,k} - \left(\frac{\partial \Phi}{\partial \boldsymbol{U}}\right)^{-1} \Phi\left(\boldsymbol{U}_{j,k}\right), \tag{11}$$

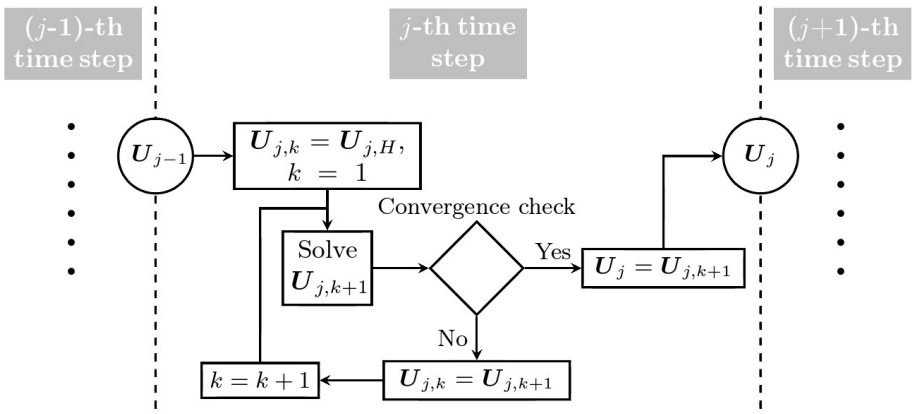

Fig. 4 Iterative procedure for Newton's method.

where k is the iteration index and the Jacobian matrix $\partial\Phi/\partial\boldsymbol{U}$ is given by

$$\frac{\partial \boldsymbol{\Phi}}{\partial \boldsymbol{U}} = \boldsymbol{I} - \left[\Delta t \left(\boldsymbol{Q} + \frac{\partial \boldsymbol{Q}}{\partial \boldsymbol{U}}\right) + \boldsymbol{U}_{j,H} - \boldsymbol{U}_{j-1}\right]. \tag{12}$$

Therefore at the beginning of the j-th time step, the homogeneous solution $\boldsymbol{U}_{j,H}$ is determined by the aeroacoustic model only and then substituted into Equation 11 as initial estimate $\boldsymbol{U}_{j,k=1}$ to start the iteration. The iteration continues until the relative error between two consecutive solution estimates satisfies

$$\frac{|\boldsymbol{U}_{j,k+1} - \boldsymbol{U}_{j,k}|}{|\boldsymbol{U}_{j,k+1}|} < \varepsilon,$$

where ε is the precision requirement and set equal to 10^{-10} in the present study.

Estimates of $p_{\text{panel},a}$ and $p_{\text{panel},b}$ are required for determining the pressure gradients $\partial p/\partial y$ in source term $\boldsymbol{Q}$ above and beneath the panel so that Equation 2 can be solved. According to Figure 3, we have

$$\left(\frac{\partial p}{\partial y}\right)_a = \frac{p_a - p_{\text{panel},a}}{l_a}, \quad \left(\frac{\partial p}{\partial y}\right)_b = \frac{p_{\text{panel},b} - p_b}{l_b}, \tag{13}$$

The two p_{panel} quantities may be calculated with Equation 6 in the form

$$p_{\text{panel},a} = p_a + \rho_a l_a \frac{\partial^2 w}{\partial t^2} \quad \text{and} \quad p_{\text{panel},b} = p_b - \rho_b l_b \frac{\partial^2 w}{\partial t^2}, \tag{14}$$

which, after combining with the discretized form of Equation 2, results in expressions in terms of elements of solution vector $\boldsymbol{U}_j$ as follows,

$$\left(\frac{\partial p}{\partial y}\right)_a = -\frac{1}{l_a}\left[\frac{1}{1+B'}\left(-p_a + p_b + B'_0\right)\right], \quad \left(\frac{\partial p}{\partial y}\right)_b = \frac{U_{1,a,k}}{U_{1,b,k}}\left(\frac{\partial p}{\partial y}\right)_a, \tag{15}$$

where

$$B' = \frac{1}{l_a U_{1,a,k}} \left\{ l_b U_{1,b,k} - \rho_p h_p - \frac{dt}{2} \left[C + \frac{4}{3} \left(\frac{\mu_a}{l_a} + \frac{\mu_b}{l_b} \right) \right] - \frac{dt^2}{4} K \right\},$$

$$B'_0 = \frac{4}{3} \left(\frac{\mu_a}{l_a} \frac{U_{3,a,k}}{U_{1,a,k}} + \frac{\mu_b}{l_b} \frac{U_{3,b,k}}{U_{1,b,k}} \right) - \left[C + \frac{4}{3} \left(\frac{\mu_a}{l_a} + \frac{\mu_b}{l_b} \right) \right] \left[\frac{dt}{2} \left(\frac{\partial^2 w}{\partial t^2} \right)^{j-1} + \left(\frac{\partial w}{\partial t} \right)^{j-1} \right]$$
$$- K \left[\frac{dt^2}{4} \left(\frac{\partial^2 w}{\partial t^2} \right)^{j-1} + dt \left(\frac{\partial w}{\partial t} \right)^{j-1} + w^{j-1} \right] - D \frac{\partial^4 w}{\partial x^4} + (T_x + N_x) \frac{\partial^2 w}{\partial x^2},$$

$$p_a = (\gamma - 1) \left[U_{4,a,k} - \frac{1}{2U_{1,a,k}} \left(U_{2,a,k}^2 + U_{3,a,k}^2 \right) \right], \; p_b = (\gamma - 1) \left[U_{4,b,k} - \frac{1}{2U_{1,b,k}} \left(U_{2,b,k}^2 + U_{3,b,k}^2 \right) \right].$$

That way the influence of panel dynamics is fully embodied into the coupled Equation 3 and the aeroacoustic-structural interaction of the panel can be accurately resolved. The details of the derivation is referred to Fan [15]. In the case of stationary fluid below panel, the normal pressure gradient can be simplified as

$$\left(\frac{\partial p}{\partial y} \right)_a = - \frac{U_{1,a,k}}{l_a U_{1,a,k} - B''} \left(-p_a + B''_0 \right), \tag{16}$$

where

$$B'' = \rho_p h_p + \frac{dt}{2} \left(C + \frac{4\mu_a}{3l_a} \right) + \frac{dt^2}{4} K,$$

$$B''_0 = \frac{4}{3} \frac{\mu_a}{l_a} \frac{U_{3,a,k}}{U_{1,a,k}} - \left(C + \frac{4}{3} \frac{\mu_a}{l_a} \right) \left(\frac{dt}{2} \left(\frac{\partial^2 w}{\partial t^2} \right)^{j-1} + \left(\frac{\partial w}{\partial t} \right)^{j-1} \right)$$
$$- K \left(\frac{dt^2}{4} \left(\frac{\partial^2 w}{\partial t^2} \right)^{j-1} + dt \left(\frac{\partial w}{\partial t} \right)^{j-1} + w^{j-1} \right) - D \frac{\partial^4 w}{\partial x^4} + (T_x + N_x) \frac{\partial^2 w}{\partial x^2} + p_0.$$

In the above expressions, the velocity gradients for determining normal stresses τ_{yy} in the forcing term in Equation 2 can be estimated with the help of tangency condition so that on the two interfaces,

$$\left(\frac{\partial v}{\partial y} \right)_a = \frac{1}{l_a} \left(v_a - \frac{\partial w}{\partial t} \right), \quad \left(\frac{\partial v}{\partial y} \right)_b = \frac{1}{l_b} \left(\frac{\partial w}{\partial t} - v_b \right). \tag{17}$$

With all the aforementioned estimations in place the source term $\boldsymbol{Q}$ can be expressed as a function of $\boldsymbol{U}_j$ and Equation 2 is ready to solve.

3. Boundary conditions

All solid surfaces are required to satisfy the tangency condition and isothermal condition $T = T_0$. For no-slip rigid surfaces, fluid have to stop on its surface so $u = v = 0$. In the CE/SE method, the boundary condition is enforced by setting ghost points. The near wall approach [16] is applied to determine the ghost point (A_G in Figure 3(b)) setting for the fluid-panel interface. Therefore the normal velocities and pressures at the ghost points, with subscript "G", are set the same as that at the fluid-panel interface, $u_G = 0$, $v_G = \partial w/\partial t$ and $p_G = p_{\text{panel}}$. The density can also be determined by the ideal gas law, $\rho_G = \gamma p_G/T_0$. All tangential gradients are simply assumed to be the same as that in the corresponding boundary point, $\boldsymbol{U}_{x,G} = \boldsymbol{U}_x$. All normal gradients are determined by linear approximation, $\boldsymbol{U}_{y,G} = (\boldsymbol{U} - \boldsymbol{U}_G)/2\delta$. One should note that these ghost point settings for the interface are aimed to calculate $\boldsymbol{U}_{j,H}$, the final aeroacoustic-structural response is corrected by the iterative procedure in Section III B 2 without involving the ghost point. At the edges of elastic panel, pinned conditions are specified.

IV. Results and Discussions

In this section we present a comparison of the effectiveness of the two aforementioned coupling schemes in resolving aeroaoustic-structural interaction problems. The solution accuracy and computational time required for solution time-marching are evaluated. All calculations are carried out after mesh convergence test [1].

A. Acoustic-structural interaction of a membrane

This problem involves the response of a single tensioned elastic membrane installed inside in a long duct when it is exposed to an acoustic wave at fixed frequency, and the acoustic transmission loss it creates. The physical configuration can be envisaged as one in Figure 1 that all cavities are removed and the top duct wall is made entirely rigid. The duct flow velocity $\hat{U}$ is set to zero so only acoustic-structural interaction is possible. Huang [7] presented a detailed linear analysis in frequency-domain of the effect of panel length on transmission loss. His theoretical solution is adopted as reference for the present comparison. The physical parameters of the problem are set as the following: the duct width $\hat{H} = 100$ mm, panel density $\hat{\rho}_p = 1000$ kg/m^3, the panel thickness

Table 1 Comparison of numerical results. $\Delta TL = |TL - TL_{reference}|$.

L_p/H	5				3.4			
	TL (db)	ΔTL (db)	T_{comp} (second)	N_{iter}	TL (db)	ΔTL (db)	T_{comp} (second)	N_{iter}
Reference (Theory)	15	—	—	—	2.5	—	—	—
Partitioned scheme	14.8	0.2	0.03415	18	1.8	0.7	0.03810	18
Monolithic scheme	14.7	0.3	0.01695	4	2.7	0.2	0.01710	3

$\hat{h}_p = 0.05$ mm, the tension $\hat{T}_x = 58.0601$ N/m, the frequency of incident wave $\hat{f} = 340$ Hz and the mean flow speed $\hat{u}_0 = 0$ m/s. $\hat{L}_0$ = panel length $\hat{L}_p$, ambient acoustic velocity $\hat{c}_0 = 340$ m/s, time $\hat{t}_0 = \hat{L}_0/\hat{c}_0$, ambient density $\hat{\rho}_0 = 1.225$ kg/m^3, pressure $\hat{\rho}_0\hat{c}_0^2$, and ambient temperature $\hat{T}_0$ are chosen for the normalization of all flow and panel variables. Fan et al. [1] studied the same problem numerically using partitioned scheme. Their results are also included in the comparison. All numerical settings of the present calculation follow those given in Fan et al. [1]. The duct lengths of panel upstream L_u and downstream L_d are set as 36 to ensure there are sufficient lengths for the generated acoustic waves to propagate. In addition, the inviscid assumption and sliding wall condition are applied. Since flow is absent in this problem, the convective term (in Equation 5) is neglected in the coupled fluid-panel equation as the same in Huang's [7] theory. The quantities D, N_x and K_p in Equation 2 are also set to zero so as to degenerate the panel equation to a membrane equation. That way ensures consistent comparison with the results of Huang [7] and Fan et al. [1]. Two calculations with membrane lengths $L_p/H = 3.4$ and 5, corresponding to a low and a high transmission loss cases respectively, are attempted.

The comparison in Table 1 shows both coupling schemes give similar accuracy in capturing high TL response. However, the accuracy of monolithic scheme solution in capturing low TL response appears to be substantially higher and the superior resolution of coupling of monolithic scheme is evident. The same two cases are also used for comparing the calculation efficiency of both schemes by inspecting two parameters, namely the wall-clock time T_{comp} required for marching a single time step during time-stationary numerical solution and the number of iteration N_{iter} incurred within the time step. The monolithic scheme gives a N_{iter} consistently smaller than the corresponding

partitioned value by at least 80% for all cases. Its T_{comp}, however, gets an approximately 50% reduction due to slightly more complicated processing involved in every iteration. Evidently the calculation efficiency of monolithic scheme doubles that of partitioned scheme.

B. Flow-induced vibration of an elastic panel in a flow duct

For all practical flows, the viscous effect on the flow-induced vibration of the elastic panel must be correctly captured numerically or else the panel may be driven to wrong vibration modes which radiate wrong acoustic waves. An example is presented and illustrated in the work of Fan et al. [17]. This capability of the coupling schemes are assessed with the extent of replicating the experimental study of flow-induced structural instability in a flow duct carried out by Liu [18]. His test rig configuration is similar to that in the previous subsection except that now the panel is backed by a cavity as deep as duct width and there is no acoustics involved. The physical parameters of the problem are set as the following: the panel length $\hat{L}_p = 300$ mm, the duct width $\hat{H} = 100$ mm, the upstream and downstream length are $\hat{L}_u = 1250$ and $\hat{L}_d = 750$ mm respectively, the panel density $\hat{\rho}_p = 7800$ kg/m^3, the panel thickness $\hat{h}_p = 0.025$ mm, the panel Young's modulus $\hat{E}_p = 193$ GPa, the panel bending stiffness $\hat{D} = 0.0002762$ Nm, the panel tension $\hat{T}_x = 40$ N and the mean flow speed $\hat{U} = 35$ m/s giving a Mach number = 0.10. The normalization is the same as the last problem. The no-slip wall condition is applied so the convective term is naturally vanished.

Figure 5a shows the comparison of time histories of the panel and flow responses obtained from the two schemes. It is surprising to observe that partitioned scheme fails to march the solution to convergence. The panel location at $x = -0.41$ is chosen because it always gives strongest vibrating velocity before time marching breaks down. It shows that a sudden change occurred the partitioned scheme solution begins to diverge at around $t = 15$ and the amplitude grew to infinity afterwards. The solution divergence is driven by a wrong estimate of panel driving pressure contaminated by the error in coupling (Figure 5b). Solving the aeroacoustic response to the panel motion in each iteration step totally relies on projecting the panel velocity and pressure on the ghost points linearly. However, the estimation of shear velocity gradient and viscous stresses on the interface may be incorrect. Through the iterative procedure, the error may be accumulated

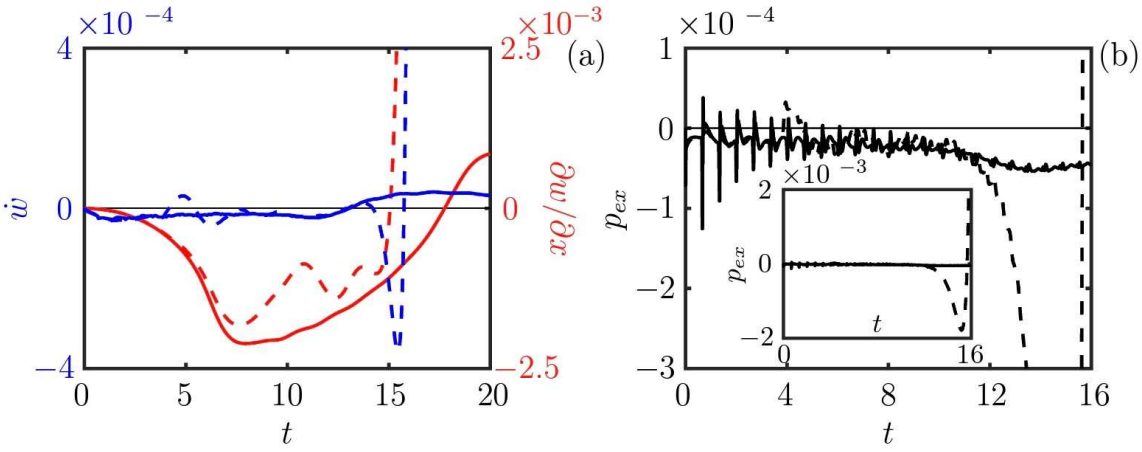

Fig. 5 Time histories of the panel and flow responses at $x = -0.41$. (a), the panel response. (b), the fluid force exerted on the panel with a zoom view in the smaller figure. – – –, result by the partitioned scheme; ——, result by the monolithic scheme.

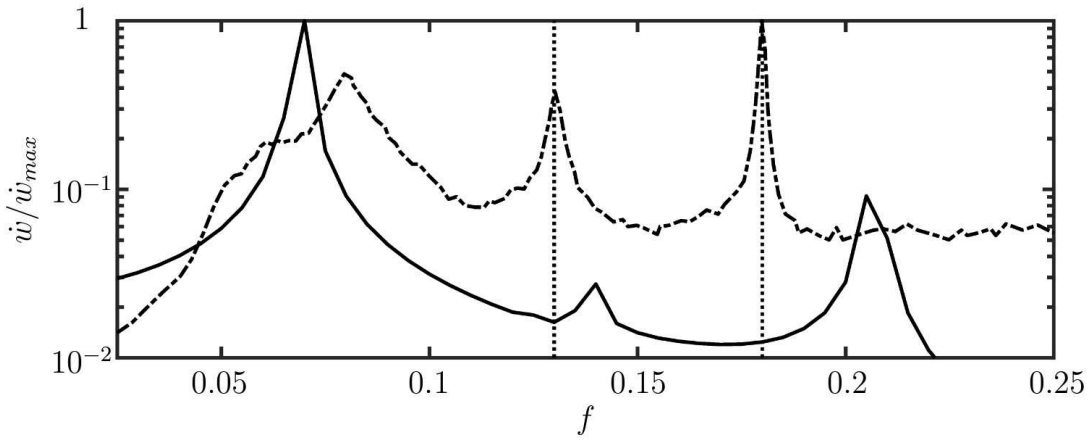

Fig. 6 Normalized frequency spectrum of the vibration velocity. ——, numerical result; –·–·–, experimental data [18]. ·····, duct mode frequencies.

and cause calculation break down. For the inviscid problem, viscous stresses vanish so this scheme is still workable. On the other hand, the monolithic scheme does not have such problem because the calculation of the iterative procedure is totally based on the actual fluid solution within the physical domain. The scheme shows a favorable agreement with the experimental data. Figure 6 shows a comparison of experimental and numerical, with monolithic, vibration velocity spectra normalized by respective maximum. A dominant peak at $f = 0.07$, together with its first and

second harmonies, are resolved in the monolithic numerical solution. The dominate peak shows a $\sim 13.5\%$ shift from the experiment. The difference may be attributed to the three dimensionality of the experiment that could not nicely be approximated in two dimensional calculation. The lack of vibration freedom along direction normal to x-y plane tends to promote panel resonant vibrations at low frequencies as easily seen from existing theoretical solutions [19]. Besides, there are another two peaks at $f = 0.13$ and 0.18 observed in the experiment but not found in the calculation. Following the theoretical analysis given by Fan et al. [17], they are found related to the excitation of wind tunnel duct acoustic modes.

C. Aeroacoustic-structural interaction of the drumlike silencer

The ability of the monolithic scheme in solving aeroacoustic-structural interaction in realistic situation is verified by replicating the experimental study of the transmission loss of a drumlike like silencer installed in a low-speed duct carried out by Choy and Huang [10]. Note that the partitioned scheme is also failed in this problem when the viscous effect is involved. The configuration of the experiment is exactly the same as shown in Figure 1. The physical parameters of the problem are set as the following: the panel length $\hat{L}_p = 500$ mm, the duct width $\hat{H} = 100$ mm, the upstream and downstream duct lengths are 1000 and 870 mm respectively, the panel density $\hat{\rho}_p = 6860$ kg/m^3, the panel thickness $\hat{h}_p = 0.025$ mm, the panel Young's modulus $\hat{E}_p = 182$ GPa, the panel bending stiffness $\hat{D} = 0.0002604$ Nm, the panel tension $\hat{T}_x = 8821.78$ N and the mean flow speed $\hat{U} = 15$ m/s giving a Mach number = 0.045. The range of frequency of interest goes from 20 to 1000 Hz. The normalization and boundary conditions are the same as that used in the previous subsection. A full panel equation (Equation 2) is used.

Recently, Dai and Aurégan [20] attempted to analyse a similar problem using multimodal solution technique in frequency-domain whose results can be used for comparison with the present result. A comparison of the numerical and experimental transmission loss TL is illustrated in Figure 7. Evidently the monolith scheme is able to well reproduce the overall trend of TL in the frequency range of interest. Same level of agreement is also observed with the multimodal result. This shows that the vibration of a panel in experiment is akin to a membrane. On the other hand

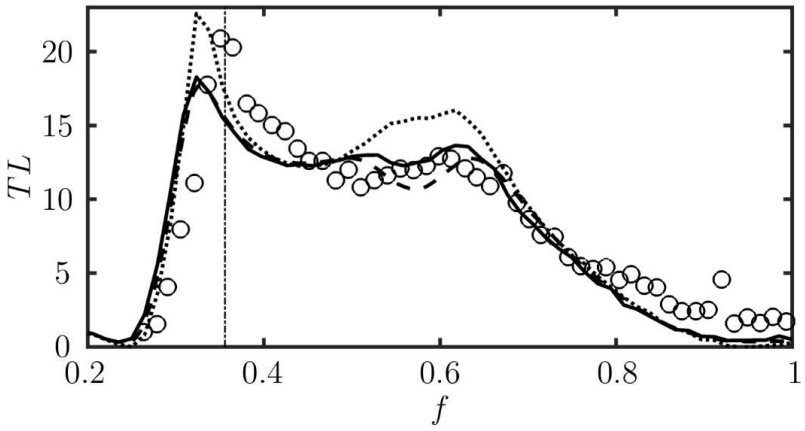

Fig. 7 Comparison of the TL spectra of numerical results and experimental data. ◯, experimental data [10]; ——, present time-marching result with full panel model; – – –, multimodal result with membrane model [20]; · · · · · ·, inviscid solution. –·–·–, duct mode frequency $f_{2,0,0}$.

a substantial under-prediction of 5 db prevails at $f \sim 0.36$. This difference can be explained by close investigation of wind tunnel duct modes [17]. In the experiment, the test section outlet is connected to a diffuser. The sudden change in area there may cause acoustic reflection. On the other hand, as confirmed in our previous study [1], the panel leading edge is responsible for the reflection of downstream going acoustic wave to upstream due to the sharp area change created by panel vibration. Reflection of upstream going wave to downstream is also possible. If we take the duct section between these two locations as an open-ended duct, it is not difficult to see that its length is 2.74 and resonates with the second duct mode frequency $f_{2,0,0} = 0.36$, which matches the observed peak in the experiment well. In the presence of this resonant mode inside the wind tunnel, the microphone was just 15 mm away from a nodal point which might receive an extremely weak acoustic signal that resulted in a highly over-estimated transmission loss. However, both the present and multimodal predictions do not suffer such duct mode contamination problem. If the data at $f = 0.36$ is ignored, the difference between numerical and experimental peak TL is only 0.5 db. In addition the monolithic scheme gives a better prediction in mid-frequencies $0.5 < f < 0.7$ than the multimodal one does. Figure 7 also shows the inviscid solution using partitioned scheme reported earlier [1]. Over-prediction of peak TL and its values within $0.5 < f < 0.7$ is evident. These observations firmly establishes the superior capability of the monolithic coupling scheme in capturing

the nonlinear aeroacoustic-structural interaction in the problem correctly. The other difference in the TL levels might be attributed to two reasons. One is due to the fact that the present two dimensional calculation does not replicate fully the three dimensionality of the experiment. Some three dimensional panel vibration and duct acoustic modal behaviours are not properly included.

V. Conclusions

This study reports on a comparison of different numerical strategies for coupling the aeroacoustics and structural dynamics of elastic panels which are flush-mounted in a flow duct and simultaneously excited by an unsteady flow and an acoustic wave. Two kinds of coupling schemes are compared, namely partitioned and monolithic schemes. The focus is put on their versatility of resolving various aeroacoustic-structural interactions and the associated accuracy and calculation time required in solution time-marching. The partitioned scheme simply solves the aeroacoustic and panel dynamic models separately and iterates their individual solutions so as to match the physical conditions on the fluid-panel interface. The aeroacoustic model is solved by conservation element and solution element (CE/SE) method whereas the panel dynamic equation is solved by standard finite difference method. The monolithic scheme treats the fluid-panel system as a single entity and includes the effects panel dynamics into an extra source term in CE/SE aeroacoustic model. Then the inhomogeneous numerical aeroacoustic model is solved with a Newton iteration method. Three cases are calculated: 1) inviscid acoustic-structural interaction of elastic panel in duct, 2) viscous flow-induced vibration of elastic panel in a flow duct, and 3) viscous aeroacoustic-structural interaction of drumlike silencer. It is found that, with the same numerical setting, both coupling schemes are able to solve the inviscid flow problem but the monolithic scheme appears to gives a more accurate solution within a much reduced calculation time. For the viscous flow problems, only the monolithic scheme produces convergent aeroacoustic-structural interaction solution but the partitioned scheme fails to do so. Furthermore, for the third case, the monolithic scheme appears able to produce a better prediction of silencer transmission loss over a wide frequency of interest than the existing multimodal result. Based on the result of the comparison, the monolithic scheme is proven an accurate and effective numerical coupling strategy for resolving the aeroacoustic-structural

interaction of an elastic panel excited by aeroacoustical flow.

Acknowledgments

The authors gratefully acknowledge the support from the Research Grants Council of Hong Kong SAR Government under Grant No. A-PolyU503/15 and the ANR/RGC international project **FlowMatAc** No. ANR-15-CE22-0016-01.

References

[1] Fan, H. K. H., Leung, R. C. K., and Lam, G. C. Y., "Numerical Analysis of Aeroacoustic-Structural Interaction of a Flexible Panel in Uniform Duct Flow," *The Journal of the Acoustical Society of America*, Vol. 137, No. 6, 2015, pp. 3115–3126.

[2] Lucey, A. D. and Carpenter, P. W., "The Hydroelastic Stability of Three-Dimensional Disturbances of a Finite Compliant Wall," *Journal of Sound and Vibration*, Vol. 165, No. 3, 1993, pp. 527–552.

[3] Sucheendran, M. M., Bodony, D. J., and Geubelle, P. H., "Coupled Structural-Acoustic Response of a Duct-Mounted Elastic Plate with Grazing Flow," *AIAA Journal*, Vol. 52, No. 1, 2014, pp. 178–194.

[4] Vitiello, P., De Rosa, S., and Franco, F., "Convected field analysis of flat panels response to turbulent boundary layer induced excitation," *Aerospace Science and Technology*, Vol. 12, No. 1, jan 2008, pp. 91–104.

[5] Schäfer, F., Müller, S., Uffinger, T., Becker, S., Grabinger, J., and Kaltenbacher, M., "Fluid-Structure-Acoustic Interaction of the Flow Past a Thin Flexible Structure," *AIAA Journal*, Vol. 48, No. 4, apr 2010, pp. 738–748.

[6] Shishaeva, A., Vedeneev, V., and Aksenov, A., "Nonlinear Single-Mode and Multi-Mode Panel Flutter Oscillations at Low Supersonic Speeds," *Journal of Fluids and Structures*, Vol. 56, 2015, pp. 205–223.

[7] Huang, L., "A Theoretical Study of Duct Noise Control by Flexible Panels," *The Journal of the Acoustical Society of America*, Vol. 106, No. 4, 1999, pp. 1801–1809.

[8] Heil, M., Hazel, A. L., and Boyle, J., "Solvers for Large-Displacement Fluid-Structure Interaction Problems: Segregated Versus Monolithic Approaches," *Computational Mechanics*, Vol. 43, No. 1, 2008, pp. 91–101.

[9] Rugonyi, S. and Bathe, K.-J., "On Finite Element Analysis of Fluid Flows Fully Coupled with Structural Interactions," *Computer Modeling in Engineering & Sciences*, Vol. 2, No. 2, 2001, pp. 195–212.

[10] Choy, Y. S. and Huang, L., "Effect of Flow on the Drumlike Silencer," *The Journal of the Acoustical Society of America*, Vol. 118, No. 5, 2005, pp. 3077–3085.

[11] Dowell, E. H., *Aeroelasticity of Plates and Shells*, Noordhoff International Publishing, Leyden, 1975, pp. 35–38.

[12] Anderson, J. D., *Fundamentals of Aerodynamics*, McGraw-Hill, New York, 5th ed., 2011, pp. 131, 146, 903–915.

[13] White, F. M., *Fluid Mechanics*, McGraw-Hill, Boston, Burr Ridge, IL, Dubuque, IA, Madison, WI, New York, San Francisco, St. Louis, Bangkok, Bogotá, Caracas, Lisbon, London, Madrid, Mexico City, Milan, New Delhi, Seoul, Singapore, Sydney, Taipei, Toronto, 4th ed., 1998, p. 572.

[14] Loh, C. Y., "Computation of Tone Noise from Supersonic Jet Impinging on Flat Plates," NASA/CR–2005-213426, AIAA-2005-0418, 2005.

[15] Fan, H. K. H., *Computational Aeroacoustic-Structural Interaction in Internal Flow with CE/SE Method*, Ph.D. thesis, Department of Mechanical Engineering, The Hong Kong Polytechnic University, Hong Kong, 2018, pp. 83–97.

[16] Lam, G. C. Y., Leung, R. C. K., Seid, K. H., and Tang, S. K., "Validation of CE/SE Scheme for Low Mach Number Direct Aeroacoustic Simulation," *International Journal of Nonlinear Sciences and Numerical Simulation*, Vol. 15, No. 2, 2014, pp. 157–169.

[17] Fan, H. K. H., Lam, G. C. Y., and Leung, R. C. K., "Numerical Study of Nonlinear Fluid-Structure Interaction of an Excited Panel in Viscous Flow," *Flinovia—Flow Induced Noise and Vibration Issues and Aspects-II: A Focus on Measurement, Modeling, Simulation and Reproduction of the Flow Excitation and Flow Induced Response*, edited by E. Ciappi, S. De Rosa, F. Franco, J.-L. Guyader, S. A. Hambric, R. C. K. Leung, and A. D. Hanford, Springer, Cham, 2019, pp. 253–269.

[18] Liu, Y., *Flow Induced Vibraion and Noise Control with Flow*, Ph.D. thesis, Department of Mechanical Engineering, The Hong Kong Polytechnic University, Hong Kong, 2011, pp. 62–77.

[19] Blevins, R. D., *Formulas for Natural Frequency and Mode Shape*, Van Nostrand Reinhold Company, New York, Cincinnati, Atlanta, Dallas, San Francisco, London, Toronto, Melbourne, 1979, pp. 252–261.

[20] Dai, X. and Aurégan, Y., "Flexural instability and sound amplification of a membrane-cavity configuration in shear flow," *The Journal of the Acoustical Society of America*, Vol. 142, No. 4, 2017, pp. 1934–1942.